Nanoscale

PAPER

View Article Online
View Journal | View Issue

Cite this: *Nanoscale*, 2026, **18**, 234

Synthesis of nucleobase-functionalized peptides and investigation on their self-assembly properties with mRNA as cargo

Jan Zimmer, Jakob Nassauer, Elena Hoffmann, Raphael Thiermann and Regina Bleul *

Received 23rd September 2025,
Accepted 25th November 2025

DOI: 10.1039/d5nr04017e

rsc.li/nanoscale

Non-covalent interactions are crucial in biological systems, *e.g.* during cell division process, assembly and desassembly of double stranded DNA. Furthermore, interactions between proteins and nucleoacids play important roles during various cell processes. This study focuses on the synthesis and characterization of thymine and lysine-bearing PEG-peptide conjugates, which leverage these interactions for nanoparticle formation. Using solid-phase peptide synthesis (SPPS), we successfully incorporated nucleobases into peptides, enabling complementary base pairing with nucleic acids. The resulting nanoparticles were characterized using transmission electron microscopy (TEM) and dynamic light scattering (DLS), confirming their uniform size and low polydispersity. We investigated the interaction of these nanoparticles with polyA-tail of mRNA. We demonstrated with the example of eGFP-mRNA, effective cellular uptake and transfection capabilities. PEGylated peptide functionalized with 6 Thymine bases, exhibited enhanced stability and transfection efficiency compared to the other variants tested. Cytotoxicity assays indicated favorable biocompatibility across various cell lines. Overall, our findings underscore the potential of nucleopeptides in developing novel gene delivery systems and advancing biotechnological applications.

Introduction

Non-covalent interactions play an important role in biological systems, particularly concerning the stability of secondary, tertiary, and quaternary structures of proteins, as well as the molecular self-assembly of nucleic acids, which is driven by complementary base pairing. Base pairing is induced through the formation of hydrogen bonds. In the context of Watson–Crick base pairing, the nucleobases adenine (A) and thymine (T) (or uracil in RNA) interact alongside guanine (G) and cytosine (C). Between A and T two hydrogen bonds are formed, while G and C engage through three hydrogen bonds, leading to a stronger interaction between G–C compared to A–T.[1,2]

The versatile properties of nucleic acids (storage of genetic information, replication, catalytic activity, formation of diverse structures, sequence-specific recognition, regulation of gene expression, and chemical modifiability) like deoxyribonucleic acid (DNA) or ribonucleic acid (RNA) have motivated the synthesis of nucleobase-bearing compounds.[2–4] Peptides or polymers containing DNA/RNA-like motifs are able to form controlled self-assembled structures, which can exhibit thermoresponsive behaviour like DNA.[5,6]

Therapeutic nucleic acids can be applied in various fields such as gene editing, protein replacement, and vaccine development. For example, in COVID-19 vaccines, the mRNA encodes an antigen, specifically a modified version of the SARS-CoV-2 spike protein, that triggers an immune response, including the production of neutralizing antibodies.[41] If nucleic acids are injected into the body, they are rapidly degraded by nucleases, which strongly limits the efficiency of the treatment.[7,8] Additionally, nucleic acids have a high molar mass and are charged negatively, which prevents them from passing the negatively charged cell membrane. Therefore, the effective transportation of therapeutic nucleic acids into target cells and efficient expression are essential. Nanocarriers encapsulating nucleic acids have to show a high transfection efficiency, low toxicity, specific targeting and good stability.[9–11]

Nucleobases can be incorporated into peptide sequences following several strategies. It is possible to integrate only the nucleobase or even nucleosides or nucleotides into the peptide. Nucleopeptides are mainly synthetic compounds that are developed for biological applications,[12] *e.g.* for the interaction with proteins or enzymes such as serum albumin[13] or the reverse-transcriptase of HIV.[14] Besides that, nucleoamino acids can be found in nature in the form of the nucleoamino acid willardiine. Willardiine is an amino acid that contains an uracil residue and occurs naturally in the seeds of *Mariosousa willardiana* and *Acacia* sensu lato.[15]

Fraunhofer Institute for Microengineering and Mikrosystems (IMM), Carl-Zeiss-Str. 18-20, 55129 Mainz, Germany. E-mail: regina.bleul@imm.fraunhofer.de

Nucleopeptides are molecules in which the peptide backbone is modified with nucleobases *via* side chain functionalities like amino or carboxy groups. They can bind to nucleic acids by complementary base pairing *via* watson–crick or hogsteen base pairing.[16]

Functionalized nucleobases can be conjugated to Fmoc-protected amino acids for the usage in solid phase peptide synthesis (SPPS). The SPPS is an elegant and well-established method to obtain nucleopeptides of a defined sequence in high yields.

Nucleopeptides can be conjugated to polyethylene glycol (PEG) to form stable nanoparticles in combination with nucleic acids. Furthermore, PEG is forming a stealth layer to mask the surface charge of the nanoparticles and prevent recognition of the reticuloendothelial system (RES) by inhibiting albumin-induced aggregation in the bloodstream.[17–19] Even with the stealth properties of PEG, the remaining positive charge on PEGylated DNA nanoparticles still facilitates protein binding in the bloodstream.[20–22]

Peptides and nucleobases can self-assemble under a variety of conditions. Therefore, nucleopeptides can show diverse self-organisation behaviour. This behaviour can be used to develop new properties and applications,[23] like tuneable or functional supramolecular architectures,[24–27] fluorescence,[28–31] to selectively sequestrate ATP in cells[32] or to deliver RNA into cells.[15,33]

In this work, we describe the synthesis and characterization of thymine and lysine bearing PEG-peptide-conjugates *via* SPPS, which should encapsulate nucleic acids efficiently and enable their cellular uptake. Therefore, the α-amino group of H-Lys(Fmoc)-OH was coupled with the carboxyl group of thymine-1-acetic acid to obtain the building block for the subsequent SPPS. Two different PEG-Peptides were synthesized and compared containing three or six thymine moieties.

We investigated the formation of nanoparticles based on the interactions of thymine and the polyA-tail of GFP-mRNA and additionally the ionic interactions between the negatively charged nucleic acid backbone and the positively charged amino group of lysine. The nanoparticles were characterized using agarose gel electrophoresis (AGE), transmission electron microscopy (TEM) and dynamic light scattering (DLS). Furthermore, the cellular uptake towards HEK-293 and cytotoxicity towards HEK-293, SCL-1 and dTHP-1 cell lines were investigated.

Results and discussion

Synthesis of amino acid building block and nucleopeptides

The α-amino group of H-Lys(Fmoc)-OH was coupled with the carboxyl group of thymine-1-acetic acid to obtain the building block for the subsequent SPPS (Fig. 1). Therefore, a simple amidation reaction using DCC/NHS as the coupling reagents was utilized. Preactivating thymine-1-acetic acid with the coupling reagents greatly improved the product yield by reducing the likelihood of self-reaction of the amino acid. The product was characterized using ^{1}H-NMR and ESI-LC-MS. Subsequently, two peptides, containing 3 or 6 thymine-lysine derivatives (T), were

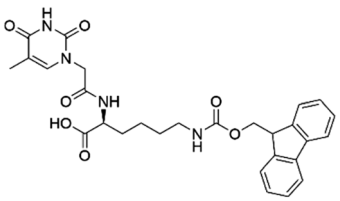

Fig. 1 Lysine-thymine-derivative as a building block for SPPS.

successfully synthesized *via* SPPS following the Fmoc-protocol using Rink Amide AM resin. The amino acid lysine (K) was incorporated alternately with T. The coupling reagents were HBTU, HOBT and DIPEA. DMF was used as the solvent.

The corresponding amino acids were used in 3.8 equivalents, HBTU and HOBT in 4 equivalents and DIPEA in an 8 equivalents excess. The amino acids were used in an excess compared to the coupling reagents to prevent guanidation, which leads to the termination of the peptide chain and minimizes the yield.[34] The deprotection of the Fmoc-group was carried out with 20% piperidine in DMF. The peptides were coupled with a N-terminal cysteine to enable them for a thiol-en reaction with maleimide functionalized polyethylene glycol monomethyl ether (mPEG-Mal) with molecular weights of 1000, 2000, 5000 or 10 000 g mol^{-1}, respectively. Finally, acetyl capping was performed to prevent side reactions during PEGylation, such as thiazine formation.[35] The peptides were cleaved from the resin using a cleavage cocktail that consisted of 90% TFA, 2.5%TIPS, 5% EDT and 2.5% water. The resin was filtered off and washed several times with TFA. The filtrate was precipitated in ice-cold diethyl ether, centrifuged and decanted to obtain the solid. This procedure was repeated twice. The solid was lyophilised and analyzed *via* ESI-LC-MS. The coupling of the thiol containing peptide and mPEG-Mal was carried out in 1× PBS pH 7.4 overnight. The progress of the reaction was monitored by ESI-LC-MS. The crude product was purified using preparative HPLC and characterized *via* HPLC and ESI-LC-MS. The obtained peptide sequences were PEG-CKKKTKKKTKKKT (**PEG-3T**) and PEG-CKTKTKTKTKTKT (**PEG-6T**) with cysteine C, lysine K and the thymine-lysine derivative T. The peptides are shown in Fig. 2. The two peptide motifs were specifically designed to investigate the role of lysine and lysine-thymine patterning in peptide structure and function, particularly in the context of charge distribution,

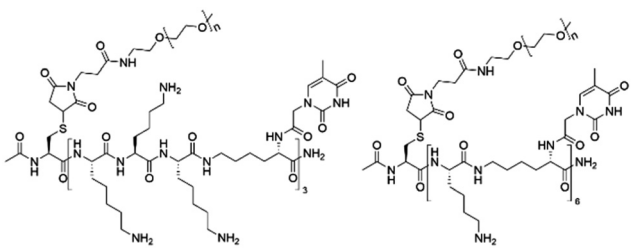

Fig. 2 Peptides synthesized *via* SPPS. PEG-CKKKTKKKTKKKT (**PEG-3T**, left) and PEG-CKTKTKTKTKTKT (**PEG-6T**, right).

and potential interactions with nucleic acids for nanoparticle formation. Linking the nucleobase to the ε-NH_2 group extends the peptide backbone, thereby increasing the spacing between nucleobases to more closely resemble the structure of nucleic acids, especially for **PEG-6T**.

Synthesis and physicochemical characterization of PEG-peptide/polyA nanoparticles

The incorporated thymine should allow the peptides to form nanoparticles, through hydrogen bonds *via* Watson–Crick base pairing, with adenine containing molecules, like the polyA-tail of mRNA. Furthermore, lysine as a cationic residue, should interact *via* ionic interactions with the negatively-charged nucleic acid backbone. To observe this behaviour, initial experiments were carried out with the single stranded RNA homopolymer polyA. To determine the necessary molecular weight of PEG to form small nanoparticles, the respective peptides were dissolved in 1× PBS pH 7.4 and mixed with polyA. The solution was heated to 85 °C for 10 minutes and slowly cooled to room temperature with 1 °C min^{-1}. The solution showed a significant turbidity after cooling, indicating the formation of nanoparticles. The resulting nanoparticles were investigated using DLS. It was observed for both peptides, that the size and PDI decreased with increasing molecular weight of PEG. This could be induced through a better shielding to the outside and therefore reduced aggregation. For both peptides containing 10 000 g mol^{-1} PEG a small size and PDI of the nanoparticles could be observed with 117 nm, PDI 0.04 for **10K-PEG-3T**/polyA and 242 nm, PDI 0.03 for **10K-PEG-6T**/polyA (Fig. 3a and b). To investigate the structural nature of the nanoparticles, cryo-transmission electron microscopy (TEM) measurements were carried out. TEM measurements of the mixture **5K-PEG-3T**/polyA (Fig. 3c and d) showed vesicles, which corroborate the DLS measurements indicating an average size of approximately 250 nm for the nanoparticles. The consistent size measurements obtained from both TEM and DLS suggest the successful formation of uniform nanoparticles within this specific formulation.

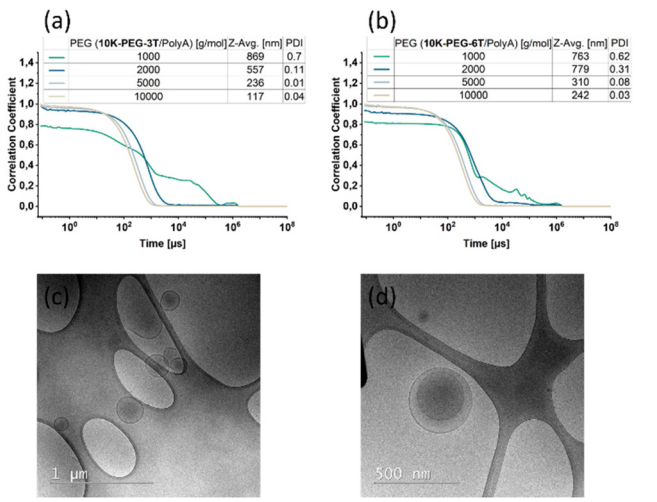

Fig. 3 DLS measurements to investigate the influence of PEG chain length on the nanoparticle formation of **PEG-3T**/polyA (a), and **PEG-6T**/polyA (b). The concentrations of **PEG-3T** and **PEG-6T** were 80 µM and the polyA concentration was 720 µM. The solvent used was 1× PBS. The table shows the mean value of the *Z*-average and the PDI of three individual measurements. Cryo-TEM images of **5K-PEG-3T**/polyA. The sizes of the scale bars are 1 µm (c) and 500 nm (d).

Agarose gel electrophoresis of PEG-peptide/EGFP nanoparticles

After experiments with polyA confirmed the possibility to form peptide/mRNA nanoparticles, further experiments were carried out using a functional GFP-mRNA. GFP-mRNA should enable the possibility to observe cellular uptake of the nanoparticles. Therefore, the peptides with a molecular PEG weight of 10 000 g mol^{-1}, that showed the smallest size and PDI in the previous experiments were mixed in different molar ratios with EGFP-mRNA. Agarose gel electrophoresis was carried out for **10K-PEG-3T**/EGFP and **10K-PEG-6T**/EGFP to determine the N : P-ratio which was necessary for complete charge compensation of the mRNA. Therefore, the RNA concentration was kept constant at 0.6 mg ml^{-1}, while the concentration of **10K-PEG-3T** and **10K-PEG-6T** was varied (Fig. 4a and b). The RNA ladder and free EGFP-mRNA were used for comparison. The EGFP-mRNA was applied to check its integrity. It was observed that a complete compensation of the negative charge could be achieved at an N : P-ratio of 1.8 : 1 for **10K-PEG-3T**/EGFP. Due to the compensated charge, the mRNA no longer penetrated the gel and remained in the pocket.[37] In addition, free EGFP-mRNA was

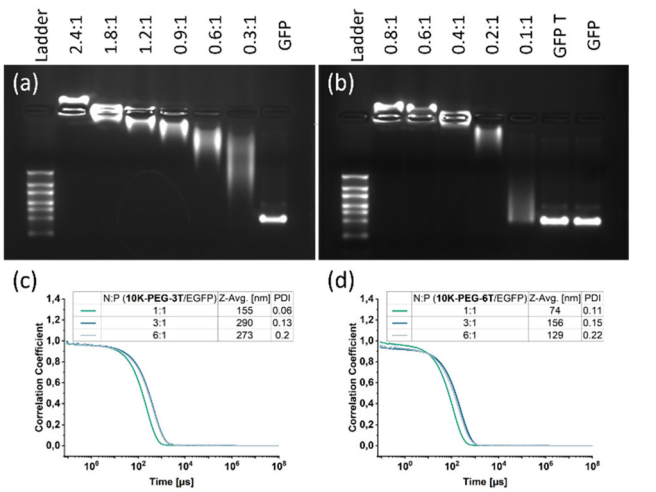

Fig. 4 Agarose gel electrophoresis to determine the N : P-ratio for complete charge compensation of the mRNA of **10K-PEG-3T**/EGFP (a) and **10K-PEG-6T**/EGFP (b). The concentration of EGFP-mRNA was 0.6 mg ml^{-1} in each case and that of the peptide was varied. The solvent used was 1× PBS. DLS measurements to analyse the N : P-ratios of **10K-PEG-3T**/EGFP (c), and **10K-PEG-6T**/EGFP (d). The concentrations of **10K-PEG-3T** and **10K-PEG-6T** were kept constant at 200 µM and the EGFP concentration was varied. The solvent used was 1× PBS. The table shows the mean value of the *Z*-average and the PDI of three individual measurements.

applied, which was heated to 85 °C for 10 minutes (GFP T) to investigate whether it was stable under the conditions required for particle formation of the EGFP-mRNA mixtures. A complete compensation of the charge could already be observed at an N : P-ratio of 0.4 : 1. The differences in the observed N : P-ratios of the two peptide/EGFP mixtures can probably be attributed to the different number of thymine bases in the peptides and their interaction with the mRNA. While the peptide **10K-PEG-3T** contained only three thymines, **10K-PEG-6T** had six thymines. However, the latter showed a lower N : P-ratio, which was necessary to compensate for the negative charge of the mRNA. This suggests that the nucleobase interaction has a major influence on the complexation of the mRNA and supports it significantly.

Synthesis and physicochemical characterisation of PEG-peptide/EGFP nanoparticles

Peptides with 3 or 6 thymine residues were analysed in different mixing ratios concerning hydrodynamic size and size distribution with DLS (Fig. 4). For the N : P-ratio 1 : 1 a small size and PDI could be observed for both peptide mixtures. The size of the nanoparticles of **10K-PEG-3T**/EGFP was 155 nm with a PDI of 0.06 and for the **10K-PEG-6T**/EGFP nanoparticles 74 nm with a PDI of 0.11. The size of the nanoparticles in both mixtures was between 70 and 200 nm, and therefore they were of a size that, according to the literature, should facilitate effective endocytosis.[38,39] The nanoparticles of the mixtures **10K-PEG-3T**/EGFP and **10K-PEG-6T**/EGFP in a N : P-ratio of 1 : 1 were also examined using cryo-TEM (Fig. 5). The images of the **10K-PEG-3T**/EGFP nanoparticles showed small spherical particles with a faintly visible membrane in the range of 70–80 nm, but also larger ones, which had a size of 120–130 nm. The images of **10K-PEG-6T**/EGFP showed larger particles in the 60–70 nm range, but also some smaller ones in the 40–50 nm range. The individual particles were well separated from each other. The slightly smaller size could be explained by the fact that the DLS measurements determined the hydrodynamic diameter of the nanoparticles, which included not only the actual nanoparticle but also its solvate shell. Due to the low electron density of the solvate shell, it could not be observed in the cryo-TEM images. In addition, even a small number of large particles affects the average size in DLS measurements more strongly than smaller ones, which means that the significantly smaller nanoparticles cannot be detected in DLS measurements.[36]

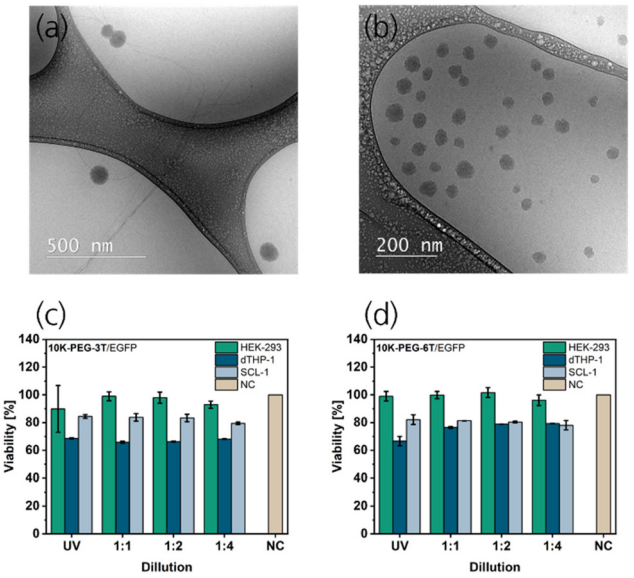

Fig. 5 TEM images of **10K-PEG-3T**/EGFP (a) and **10K-PEG-6T**/EGFP (b), both N : P-ratio 1 : 1 in 1× PBS pH 7.4. Cell viability of HEK-293 (turquoise), dTHP-1 (dark blue) and SCL-1 cells (light blue) relative to the negative control (NC, brown). Cells were treated with different ratios (undiluted (UV), 1 : 1–1 : 4) of **10K-PEG-3T**/EGFP (c) or **10K-PEG-6T**/EGFP (d) for 24 h. The error bars represent the standard deviation of the mean. Experiments were carried out as duplicates.

Cytotoxicity studies of PEG-peptide/EGFP nanoparticles

To evaluate the biocompatibility of the synthesized nanoparticles for further use in therapeutic applications, the cytotoxicity was investigated following the CCK8-assay. **10K-PEG-3T**/EGFP and **10K-PEG-6T**/EGFP nanoparticles were applied to HEK-293, SCL-1 and dTHP-1 cell lines in different dilutions (undiluted (UV), 1 : 1, 1 : 2 and 1 : 4). While HEK-293 cells were investigated due to their relevance in transfection studies, dTHP-1 and SCL-1 cells were used to demonstrate that, at a specific concentration, the carrier peptide and its associated nanoparticles did not cause any direct damage to healthy immune or cancer cells. The HEK-293 cells showed a high viability for both nucleopeptides relative to the untreated cells (NC) in all dilutions. The viability was at least 90% or higher. In addition, the results show that the viability of SCL-1 cells was at around 80% for **10K-PEG-3T**/EGFP and **10K-PEG-6T**/EGFP nanoparticles in every dilution. This indicated that the viability was still very high, and no concentration dependent toxic effects could be observed in the investigated concentration range. For dTHP-1 cells the viability was lower after the treatment with both nanoparticles. For **10K-PEG-3T**/EGFP the viability remained at 60% for all dilutions, while the viability was higher for the 1 : 2 dilution with **10K-PEG-6T**/EGFP nanoparticles at around 75%. Therefore, the results demonstrate that the nanoparticles meet the basic criteria of cellular applications.

Transfection studies of PEG-peptide/EGFP nanoparticles

After the physicochemical characterization of PEG-peptide/GFP nanoparticles, further experiments were performed to test the ability of **10K-PEG-3T**/EGFP and **10K-PEG-6T**/EGFP in nanoparticle transfection and translation of the encapsulated mRNA. Following the successful delivery into the cells and endosomal escape, EGFP-mRNA is translated into the corresponding green fluorescent protein. The fluorescence can be observed under a fluorescence microscope. **10K-PEG-3T**/EGFP and **10K-PEG-6T**/EGFP Nanoparticles were applied to HEK-293 cells to investigate their GFP expression (Fig. 6). While **10K-PEG-3T**/EGFP showed no GFP expression, **10K-PEG-6T**/EGFP nanoparticles showed successful transfection and sub-

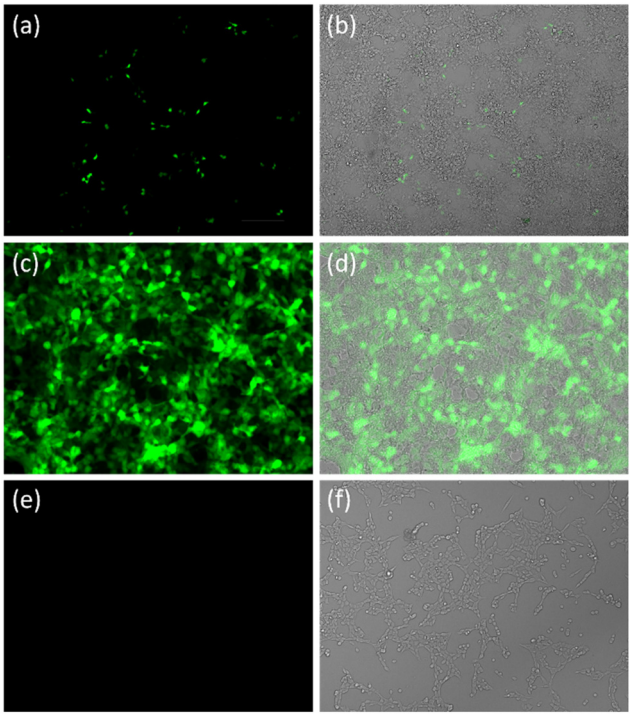

Fig. 6 Cellular uptake of nanoparticles in HEK-293 cells. Fluorescence images of **10K-PEG-6T**/EGFP N : P-ratio 1 : 1 in 1× PBS pH 7.4 (a), positive control: lipofectamine/EGFP (c), negative control: EGFP-mRNA in 1× PBS pH 7.4 (e) and corresponding overlays (b, d and f).

sequent GFP expression in HEK-293 cells 24 h after treatment. As a negative control EGFP-mRNA in PBS was used and as a positive control lipofectamine/EGFP nanoparticles were used. While the negative control showed no GFP expression, the positive control showed significantly higher GFP expression compared to the **10K-PEG-6T**/EGFP nanoparticles. However, the enhanced GFP Expression for **10K-PEG-6T**/EGFP compared to **10K-PEG-3T**/EGFP nanoparticles could be explained by the larger size of **10K-PEG-3T**/EGFP nanoparticles with around 150 nm compared to **10K-PEG-6T**/EGFP nanoparticles with around 75 nm. Therefore, a nucleobase count of 6 is necessary to ensure targeted transfection. Furthermore, this shows, that the **10K-PEG-6T**/EGFP nanoparticles are stable under physiological conditions and can release their cargo efficient following the cellular uptake. The cellular uptake is promoted by the cationic lysine residues, which can interact with the cell membrane and condensate EGFP-mRNA efficient in combination with the thymine residues. This effect is typical for cell penetrating peptides, that are usually highly charged like the HIV-TAT-peptide.[40] Furthermore the cationic part can promote endosomal escape by the proton sponge effect. The attached PEG-chain prevents aggregation and reduces the nanoparticle size for efficient transfection.[17,18]

Conclusion

In this study, we successfully synthesized and characterized thymine and lysine-bearing PEG-peptide conjugates, demonstrating their potential for nanoparticle formation through specific interactions with nucleic acids. The incorporation of thymine facilitated Watson–Crick base pairing with adenine, while lysine contributed ionic interactions with negatively charged nucleic acids, leading to effective self-assembly. Characterization techniques such as DLS and TEM confirmed the formation of uniform nanoparticles, with optimal sizes and low polydispersity indexes, particularly at higher PEG molecular weights. Furthermore, cytotoxicity studies indicated good biocompatibility of the nanoparticles across different cell lines, while transfection experiments illustrated the ability of **10K-PEG-6T**/EGFP nanoparticles to efficiently deliver RNA and express the corresponding fluorescent protein in cells. These findings highlight the promising application of nucleopeptides in gene delivery systems and other biotechnological applications.

Experimental section

The solvents Acetonitrile (ACN), dimethylformamide (DMF), methanol, pyridine and diethyl ether were obtained from Omnilab. Fmoc-protected amino acids were purchased from Carbolution Chemicals GmbH (Fmoc-Lys(boc)-OH, H-Lys (Fmoc)-OH) and BLD Pharmtech Ltd (Fmoc-Cys(Trt)-OH). Rink-Amide-AM resin (100–200 mesh, loading: 0.62 mmol g^{-1}) was obtained from Merck Millipore. Piperidine, trifluoroacetic acid (TFA), *N*,*N*-diisopropylethylamine (DIPEA), acetic anhydride and Formic Acid (FA) were purchased from Carl Roth GmbH + Co. KG. Ethane-1,2-dithiol (EDT), Triisopropylsilane (TIPS), 1-hydroxybenzotriazole (HOBT) monohydrate, and 2,4,6-Trinitrobenzenesulfonic acid (TNBS) were obtained from TCI Deutschland GmbH. Hexafluorophosphate Benzotriazole Tetramethyl Uronium (HBTU), thymine-1-acetic acid and *N*-hydroxysuccinimide (NHS) were purchased from Carbolution Chemicals GmbH. GFP-mRNA was received from Fraunhofer ITEM. Water was deionized before usage using a GenPure UV/UF xCAD system from Thermo Fisher Scientific.

Coupling of thymine to the amino acid

In a round bottom flask, thymine-1-acetic acid (3.00 g, 16.29 mmol, 1.0 eq.) and NHS (2.81 g, 24.4 mmol, 1.5 eq.) were dissolved in 50 ml DMF. DCC (3.70 g, 17.9 mmol, 1.1 eq.) was added and stirred overnight at room temperature. The DCC-urea was filtered off and the filtrate was collected in a round bottom flask. H-Lys(Fmoc)-OH (4.72 g, 12.8 mmol, 0.8 eq.) was added and DIPEA (7.44 ml, 5.52 g, 42.7 mmol, 2.6 eq.) was added dropwise. After stirring again overnight, the solution was slightly concentrated *in vacuo* and then poured into water pH 2. The colourless solid was filtered and washed several times with water. The crude product was lyophilised and purified *via* column chromatography with DCM/MeOH 9 : 1 with 1% AcOH.

Yield: 3.02 g (5.65 mmol, 35%), colourless powder.

^{1}H-NMR (300 MHz, DMSO-d_6, 296 K): δ = 11.27 (s, 1H, NH^{Thymine}); 8.43–8.36 (m, 1H, NH^{Linker}); 7.89 (d, J = 7.4 Hz, 2H,

CH^{Fmoc}); 7.69 (d, J = 7.4 Hz, 2H, CH^{Fmoc}); 7.66–7.42 (m, 6H, CH^{Fmoc}, CH^{α}, $CH^{Thymine}$); 4.39–4.11 (m, 6H, CH-CH_2^{Fmoc}, CH^{α}, CH_2^{Linker}); 3.01–2.91 (m, 2H, CH_2-NH); 1.74 (s, 3H, $CH_3^{Thymine}$); 1.71–1.10 (m, 6H, CH_2^{Lysine}).

ESI-HRMS (ACN + FA) (m/z): calculated $[C_{28}H_{31}N_4O_7]^+$: 535.3212; found: 535.3189.

Nucleopeptide synthesis

The synthesis was carried out using the Fmoc-protocol. The peptides were synthesized using Rink-Amid resin (loading: 0.62 mmol g^{-1}) in a peptide synthesis apparatus. The resin was swelled in DMF. To deblock the amino group of the resin, 20% piperidine in DMF v/v (10 ml g^{-1} resin) was added (3 × 15 min). The resin was washed 5–6 times with DMF. For preactivation of the Fmoc-protected amino acid, the corresponding amino acid (3.8 eq.), HBTU (4 eq.), HOBT (4 eq.) and DIPEA (8 eq.) were dissolved in DMF (10 ml g^{-1} resin) and kept in an ultrasonic bath for 10 min. The preactivated amino acid was added to the reaction solution and shaken for 2 to 2.5 hours. The reaction was monitored using the Kaiser and TNBS test. The resin was washed 5–6 times with DMF. Free amino groups were saturated with acetic anhydride (8 eq.) and pyridine (8 eq.) in DMF (10 ml g^{-1} resin) (1 × 15 min). It was washed 5–6 times with DMF and the procedure was repeated as often as desired, starting with deblocking of the amino group of the peptide chain on the resin. Afterwards, the peptide was cleaved from the resin. The resin was washed 5–6 times with DMF, methanol and diethyl ether and then a cleavage cocktail containing 90% TFA, 5% EDT, 2.5% TIPS and 2.5% water (v/v) (10 ml g^{-1} resin, 1 × 2 h) was added. The resin was filtered off and washed 5–6 times with TFA. The filtrate was precipitated in ice-cold diethyl ether, centrifuged and decanted to obtain the solid. This procedure was repeated twice. The solid was lyophilised and analyzed *via* analytical LC-MS (Fig. S2).

PEG-conjugation

Peptide-SH (1 eq.) was dissolved in 1× PBS pH 7.4 (1.5 ml). mPEG-Mal (1.1 eq.) was also dissolved in 1× PBS pH 7.4 (0.8 ml) and added to the peptide. The solution was stirred overnight. The solution was taken up in a syringe and injected into the preparative HPLC. The purified peptides were characterized by analytical LC-MS (Fig. S3 and S4).

RP-HPLC

The analytical HPLC was performed on an Agilent 1260 Infinity II system from Agilent Technologies. The system consisted of a quaternary pump, an in-line degasser, a multisampler, a column oven and a diode array detector (DAD). The system was controlled with the MassHunter Workstation LC/MS Data Acquisition v.10.1 software. The MassHunter Workstation Qualitative Analysis v.10.0 software was used for analysis. InfinityLab Poroshell column (120 EC-C18 3.0 × 150 mm, 2.7 μm) from Agilent Technologies was used as stationary phases and water and ACN with 0.1% FA each were used as mobile phases. Typical gradients were run from 5% to 100% ACN. The separations were carried out at 40 °C.

The preparative HPLC was carried out on a puriFlash 5250P from Advion Interchim Scientific. The system consisted of a quaternary pump, an in-line degasser, a UV/VIS detector, a single quadrupole mass spectrometer, a light scattering detector (ELSD) and a fraction collector. The sample was injected through a 2.5 ml or 5.0 ml sample loop. The InterSoft X software was used for control and data evaluation. The columns Uptisphere Strategy C18-HQ 10 μm 250 × 21.2 mm and Utisphere Strategy C18-HQ 5 μm 150 × 10 mm from Interchim were used as stationary phases and water and ACN with 0.1% TFA each were used as mobile phases. Typical gradients were run from 5% to 100% ACN over one hour. The separations were carried out at room temperature.

Mass spectrometry

The mass spectrometry measurements were carried out on an Agilent 6530 QTOF-MS from Agilent Technologies. Electrospray ionisation (ESI) was used. The system was controlled with the software MassHunter Workstation LC-MS Data Acquisition v.10.1. The MassHunter Workstation Qualitative Analysis v.10.0 software was used for evaluation.

DLS measurements

To investigate the hydrodynamic particle size and the polydispersity index (PDI) of nanoparticles, DLS measurements were carried out using a Zetasizer Ultra from Malvern Panalytical. The measurements were performed at 25 °C and an equilibration time of 120 seconds. The measurements were carried out undiluted. The measurements were analysed and exported using the software ZS Xplorer v.3.3.1.5.

Self-assembly of PEG-peptide/EGFP-mRNA nanoparticles

The self-assembly of PEG-peptide/EGFP-mRNA nanoparticles was performed by pipette mixing of 50 μl of PEG-peptide (400 μM) in 1× PBS pH 7.4 with 50 μl of EGFP-mRNA (2.4 mM, 1.2 mM or 400 μM) in 1× PBS pH 7.4. The solution was heated at 85 °C for 10 minutes and slowly cooled to room temperature. A turbid solution indicated nanoparticle formation.

TEM measurements

Cryogenic TEM imaging was performed on lacey carbon-coated copper grids using a Zeiss Libra 120 under cryogenic conditions. Before use, the grids were made hydrophilic *via* oxygen plasma treatment. A 5 μL droplet of the sample suspension was applied to each grid, excess liquid was removed with filter paper, and the grid was then immediately vitrified in liquid ethane at −180 °C using a Leica EM GP. The grids were stored in liquid nitrogen before being transferred to the electron microscope. Imaging was carried out at 120 kV using a Gatan UltraScan® CCD camera. Vitrified grids were loaded into the microscope *via* a Gatan cryostage, which maintained temperatures below −170 °C. Images were acquired across multiple magnifications to assess the specimen's overall distribution.

Cellular uptake

Human Embryonic Kidney (HEK-293) cells were cultured in Dulbecco's Modified Eagle's medium (DMEM) supplemented with 10% FBS + 1% Pen/Strep. All cells were cultured in a humidified incubator, containing 5% CO_2 at 37 °C. HEK-293 cells growing in 96 well plates at the density of 10^4 cells per well for 24 h were treated with Nucleopeptide/GFP-mRNA nanoparticles for 24 h by culture media change and direct addition of NPs to the media. The cells were analysed by a Keyence confocal microscope (BZ-X-800).

Cytotoxicity-assay

HEK-293 cells were cultured according to the procedure described above. Squamous Cell Carcinoma (SCL-1), kindly provided by Dr Petra Boukamp (DKFZ, Heidelberg, DE) were cultivated in DMEM low glucose (Gibco), 10% (v/v) fetal calf serum and 1% Penicillin/Streptomycin. THP-1 cells were kindly provided by Dr Nico Lachmann (Fraunhofer Institute for Toxicology and Experimental Medicine ITEM, DE) and cultured in RPMI 1640 medium (Capricorn Scientific, Ebsdorfergrund, DE) with 10% (v/v) fetal calf serum and 1% Penicillin/Streptomycin. THP-1 cells were stimulated to dTHP-1 with 7.5 ng mL^{-1} phorbol 12-myristate 13-acetate (Fischer Scientific) 24 h prior treatment. For cytotoxicity testing, 10 000 HEK-293 cells, 12 000 SCL-1 cells and 100 000 THP-1 cells per well were added to a 96 well plate and cultivated and stimulated (dTHP-1) for 24 h at 37 °C and 5% CO_2. Samples were analysed in duplicates with a final concentration of 10% (v/v) in 100 µL per well. A 10% PBS solution was added as a control. After 24 h the medium was removed and a 10% (v/v) working solution of a Cell Counting kit-8 (Sigma Aldrich) added according to manufacturer's specifications. Cells were incubated for 2 h at 37 °C and absorbance was measured at 450 nm using a Spark Plate Reader (Tecan).

Agarose gel electrophoresis

A 1.2% agarose gel was prepared by dissolving 1.2 g agarose in 100 ml TBE buffer (Tris-Borate-EDTA). The solution was heated in a microwave until the agarose was completely dissolved. The gel was then poured into the gel chamber with 8 pockets and cooled to room temperature. To analyse the peptide/EGFP samples, 3 µl of the peptide/EGFP sample was mixed with 3 µl of 2× RNA Loading Dye. The samples were adjusted to an EGFP concentration of 0.6 mg ml^{-1}. A Riboruler High Range RNA ladder with 200 to 6000 bases from Thermo Scientific was used. For this, 6 µl of the ladder was mixed with 6 µl of 2× RNA Loading Dye. The mixtures were heated at 70 °C for 10 minutes and then placed on ice to prevent renaturation. 5 µl of the peptide/EGFP samples and 10 µl of the ladder were applied. Electrophoresis was performed under an applied voltage of 120 V for a period of 45 minutes. The agarose gel was then viewed under UV light to analyse the bands of the peptide/EGFP samples.

Author contributions

J. Z. conceived and designed the experiments. J. Z. synthesized the amino acids and nucleopeptides and carried out analysis and purification with HPLC and LC-MS and nanoparticle formulation. J. Z. carried out DLS measurements. R. T. carried out TEM measurements. E. H. carried out AGE measurements. J. N. carried out cytotoxicity- and cellular uptake-assays. R. B. supervised the work, administrated the project, gained project funding. All authors have read and agreed to the published version of the manuscript.

Conflicts of interest

There are no conflicts to declare.

Data availability

All data presented in our article are either included in the manuscript directly or provided in the article's supplementary information (SI). Supplementary information: Fig. S1–S5. See DOI: https://doi.org/10.1039/d5nr04017e.

Acknowledgements

We would like to express our gratitude for the financial support of the BioTherNa (13XP5113) junior research group by the Federal Ministry of Education and Research (BMBF) and the funding by the Fraunhofer Lighthouse Project RNAuto. Their contributions were instrumental in the successful execution of our research.

References

1 M. Meot-Ner, *Chem. Rev.*, 2005, **105**, 213–284.
2 S. Sivakova and S. J. Rowan, *Chem. Soc. Rev.*, 2005, **34**, 9–21.
3 T.-H. Le, Y. Kim and H. Yoon, *Polymers*, 2017, **9**, 150.
4 R. McHale and R. K. O'Reilly, *Macromolecules*, 2012, **45**, 7665–7675.
5 J. F. Lutz, F. Thünemann and K. Rurack, *Macromolecules*, 2005, **38**, 8124–8126.
6 S. Chea, K. Schade, S. Reinicke, R. Bleul and R. R. Rosencrantz, *Polym. Chem.*, 2022, **13**, 5058–5067.
7 F. Alaee, *et al.*, *Gene Ther.*, 2014, **21**, 139–147.
8 Y. Huang, *et al.*, *Mol. Ther.*, 2011, **19**, 381–385.
9 J. Yang and G.-F. Luo, *Chemistry*, 2023, **5**, 1696–1718.
10 M. Zhang, X. Guo, M. Wang and K. Liu, *J. Controlled Release*, 2020, **323**, 203–224.
11 P. Midoux, C. Pichon, J. J. Yaouanc and P. A. Jaffrès, *Br. J. Pharmacol.*, 2009, **157**, 166–178.
12 P. L. Scognamiglio, C. Platella, E. Napolitano, D. Musumeci and G. N. Roviello, *Molecules*, 2021, **26**, 3558.

13 G. N. Roviello, G. Oliviero, A. Di Napoli, N. Borbone and G. Piccialli, *Arabian J. Chem.*, 2020, **13**, 1966–1974.
14 G. N. Roviello, S. Di Gaetano, S. Franco, *et al.*, *J. Med. Chem.*, 2011, **54**, 2095–2101.
15 T. Giraud, P. Hoschtettler, G. Pickaert, M.-C. Averlant-Petit and L. Stefan, *Nanoscale*, 2022, **14**, 4908–4921.
16 M. E. Mercurio, S. Tomassi, M. R. Gaglione, *et al.*, *J. Org. Chem.*, 2016, **81**, 11612–11625.
17 K. Kizzire, S. Khargharia and K. G. Rice, *Gene Ther.*, 2013, **20**, 407–416.
18 K. Y. Kwok, R. C. Adami, K. C. Hester, *et al.*, *Int. J. Pharm.*, 2000, **203**, 81–88.
19 S. Khargharia, K. Kizzire, M. D. Ericson, N. J. Baumhover and K. G. Rice, *J. Controlled Release*, 2013, **170**, 325–333.
20 R. J. Allen, B. Mathew and K. G. Rice, *Mol. Pharm.*, 2018, **15**, 3881–3891.
21 N. J. Baumhover, J. T. Duskey, S. Khargharia, *et al.*, *Mol. Pharm.*, 2015, **12**, 4321–4328.
22 B. Mathew, R. Ramanathan, N. A. Delvaux, *et al.*, *Gene Ther.*, 2020, **27**, 196–208.
23 T. MacCulloch, A. Buchberger and N. Stephanopoulos, *Org. Biomol. Chem.*, 2019, **17**, 1668–1682.
24 N. Gour, D. Kedracki, I. Safir, K. X. Ngo and C. Vebert-Nardin, *Chem. Commun.*, 2012, **48**, 5440–5442.
25 M. L. Daly, Y. Gao and R. Freeman, *Bioconjugate Chem.*, 2019, **30**, 1864–1869.
26 A. Chotera, H. Sadihov, R. Cohen-Luria, P.-A. Monnard and G. Ashkenasy, *Chemistry*, 2018, **24**, 10128–10135.
27 A. Buchberger, C. R. Simmons, N. E. Fahmi, R. Freeman and N. Stephanopoulos, *J. Am. Chem. Soc.*, 2020, **142**, 1406–1416.
28 N. Gour, *et al.*, *Chem. Commun.*, 2014, **50**, 6863–6865.
29 C. Diaferia, *et al.*, *Chemistry*, 2021, **27**, 14307–14316.
30 R. Bucci, A. Bossi, E. Erba, F. Vaghi, *et al.*, *Sci. Rep.*, 2020, **10**, 19331.
31 C. Avitabile, C. Diaferia, V. Roviello, *et al.*, *Chemistry*, 2019, **25**, 14850–14857.
32 H. Wang, Z. Feng and B. Xu, *Angew. Chem., Int. Ed.*, 2019, **58**, 10423–10432.
33 S. Tomassi, *et al.*, *Bioorg. Med. Chem.*, 2018, **26**, 2539–2550.
34 F. Albericio, J. M. Bofill, A. El-Faham and S. A. Kates, *J. Org. Chem.*, 1998, **63**, 9678–9683.
35 I. N. Gober, A. J. Riemen and M. Villain, *J. Pept. Sci.*, 2021, **27**, e3323.
36 S. K. Filippov, *et al.*, *Mater. Horiz.*, 2023, **10**, 5354–5370.
37 Y. Wang, *et al.*, *Colloids Surf., A*, 2020, **590**, 124529.
38 Q. Leng, Z. Imtiyaz, M. C. Woodle and A. J. Mixson, *Pharmaceutics*, 2023, **15**, 1482.
39 S. Tarvirdipour, C.-A. Schoenenberger, Y. Benenson and C. G. Palivan, *Soft Matter*, 2020, **16**, 1678–1691.
40 A. Erazo-Oliveras, N. Muthukrishnan, R. Baker, T.-Y. Wang and J.-P. Pellois, *Pharmaceuticals*, 2012, **5**, 1177–1209.
41 D. Adams, *et al.*, *N. Engl. J. Med.*, 2018, **379**, 11–21.